Effect of Mg content on the structural and optical properties of $Mg_xZn_{1-x}O$ alloys

WU ChunXia[1,2*], LU YouMing[2], SHEN DeZhen[2] & FAN XiWu[2]

[1]*Photonics Fabrication Science Center, Jiangsu University, Zhenjiang 212013, China*
[2]*Key Laboratory of Excited State Processes, Changchun Institute of Optics, Fine Mechanics and Physics, Chinese Academy of Sciences, Changchun 130033, China*

$Mg_xZn_{1-x}O$ thin films with $x = 0$, 0.11, 0.28, 0.44, 0.51, and 0.65 were grown by plasma-assisted molecular beam epitaxy on (0001) sapphire substrates. X-ray diffraction measurement reveals that phase separation of the $Mg_xZn_{1-x}O$ films occurred at $x = 0.44$ and 0.51. Optical absorption spectra show that the absorption edges of the films shift to high-energy side with increasing Mg contents. In resonant Raman spectra, multiple-order Raman peaks originating from ZnO-like longitudinal optical phonons were observed. Moreover, the blue shift and the full width at half maximum of Raman scattering peaks increase continuously with x increasing from 0 to 0.28, which indicates that Zn is substituted by Mg in hexagonal lattice.

P-MBE, $Mg_xZn_{1-x}O$ alloy films, phase separation, resonant Raman

As a direct band gap semiconductor, ZnO has attracted considerable attention due to its potential applications in ultraviolet (UV) light-emitting devices and laser devices. $Mg_xZn_{1-x}O$ alloy is considered to be a proper barrier material in ZnO-based heterostructures and related devices to realize double confinement actions for electrons and photons [1–4]. However, it is well known that MgO and ZnO are stabilized in rocksalt and wurtzite structures, respectively. Therefore, the difference in the crystalline structure between ZnO and MgO will result in phase separation at a certain Mg content. According to the phase diagram of the ZnO–MgO ternary system, the thermodynamic solubility limit of MgO in ZnO is less than 4 mol% [5]. Whereas, it has been reported that single-phased MgZnO films can be obtained with Mg compositions up to 49at% using metal organic vapor phase epitaxy (MOVPE) [6]. Recent reports have demonstrated that the solid solubility limit can be varied using different techniques [6–10]. For example, it has

been reported by Koike et al. that the solid solubility limit can be changed from $x = 0.3$ to $x = 0.45$ at different growth temperatures in molecular beam epitaxy (MBE) [7]. Fujita et al. have proposed that the use of a high-quality ZnO buffer layer would allow the growth of single-phased wurtzite $Mg_xZn_{1-x}O$ with Mg content as high as 0.51 [8]. In our experiment, it is found that the solid solubility limit of MgO in ZnO is smaller than 44at% in a plasma-assisted MBE. In previous papers, the researches on the optical properties of the MgZnO films were mainly characterized using absorption and photoluminescence measurements. So far no Raman scattering data of MgZnO alloys can be found to the best of our knowledge, although it can be much useful to determine the composition and phase transition in MgZnO alloys. In this paper, $Mg_xZn_{1-x}O$ ($0 \leqslant x \leqslant 0.65$) thin films were grown by plasma assisted molecular beam epitaxy (P-MBE). The influence of Mg content on the crystal structures and optical properties of the films was studied by XRD diffraction, absorption and Raman scattering. Multiple phonon scattering peaks of the MgZnO thin films were observed.

*Corresponding author (email: chxwu7771@yahoo.com.cn)

1 Experiment

A VG V80H MBE system with Knudsen-cells for the evaporation of Zn solid source (99.9999%) and Mg solid source (99.999%) was used for the growth of the $Mg_xZn_{1-x}O$ alloy thin films. Atomic oxygen was generated from ultrapure O_2 gas (99.999%) by a radio frequency (RF) plasma source with an electrostatic ion trap operated at 500 V. The RF power of O-plasma source was fixed at 300 W and the flow rate was kept at 2.0 sccm during growth. C-plane Al_2O_3 was used as substrate. The substrates were pretreated at 800°C in ultrahigh vacuum ($<1\times10^{-8}$ mbar) for 30 min to remove the surface contaminants. The base pressure of the growth chamber was about 1×10^{-9} mbar. During the growth, the substrate temperature was kept at 700°C, and the Zn partial pressure was kept at 4×10^{-5} mbar and the Mg partial pressures changed from 1×10^{-7} to 5×10^{-7} mbar to get a series of $Mg_xZn_{1-x}O$ with different Mg content. The atomic percentage in the MgZnO was determined by energy dispersive X-ray (EDX) spectroscopy. The thickness of the films was measured to be about 300 nm. A BRUKER D8 DISCOVER X-ray diffractometer was used for XRD measurement. The absorption spectra were carried out using an UV-360 spectrophotometer. A JY63 Micro Raman spectrometer was employed for PL and Raman scattering measurements. The excitation source was the 325 nm line of a He–Cd laser with 50 mW power. Raman scattering spectra were collected in a back-scattering geometric configuration.

2 Results and discussion

Figure 1 shows the XRD spectra of the $Mg_xZn_{1-x}O$ alloy thin films with x = 0, 0.11, 0.28, 0.44, 0.51 and 0.65, which are labeled as samples A, B, C, D, E and F, respectively. With increasing Mg content up to 0.28, only one peak corresponding to $Mg_xZn_{1-x}O$ (002) can be observed, indicating the formation of single-phased $Mg_xZn_{1-x}O$ films with hexagonal crystal structure. Similar result has been obtained by Sharma et al., who obtained hexagonal $Mg_xZn_{1-x}O$ alloy film with maximum Mg incorporation of 33at%[9]. With further increasing the Mg content, the XRD spectrum of $Mg_xZn_{1-x}O$ at x = 0.44 shows an additional peak at 36.61°, which is very close to the (111) diffraction peak of cubic MgO. It is found that the position of this peak shifts to high angle side with increasing Mg content to 51%, as shown in Figure 1E. This fact indicates the formation of cubic-structured MgZnO. The appearance of hexagonal (002) peak and cubic (111) peak indicates the occurrence of phase separation. For the Mg content of 51%, the intensity of cubic MgZnO (111) peak is stronger than that of hexagonal MgZnO (002) peak. When x equals 0.65 (sample F), only one cubic MgZnO (111) peak is observed at 36.71°, which indicates that MgZnO alloy thin film has completed the transition from wurtzite structure to cubic structure.
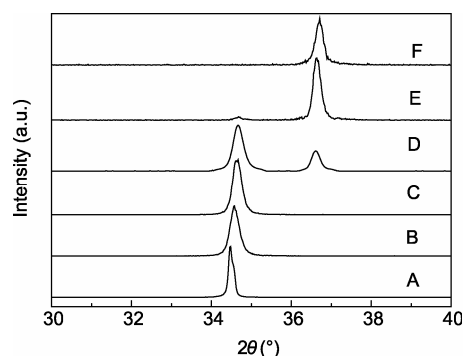

Figure 1 XRD spectra of the $Mg_xZn_{1-x}O$ thin films with different compositions. A, x=0; B, x=0.11; C, x=0.28; D, x=0.44; E, x=0.51; F, x=0.65.

The lattice constant of the samples is calculated according to the following equations: $a=\lambda/2\sin\theta\sqrt{(h^2+hk+k^2)}$, where a is lattice constant, h, k, l are miller indices, and λ and θ are X-ray wavelength (λ= 1.5418 Å) and Bragg angle, respectively. Figure 2 shows the dependences of the lattice constants and the full widths at half maximum (FWHM) for the hexagonal MgZnO (002) peak and the cubic MgZnO (111) peak on Mg composition (x) in $Mg_xZn_{1-x}O$ films. It is well known that the c-axis constant of bulk ZnO is 5.205 Å, and the lattice constant of MgO is 4.213 Å. From Figure 2(a), it can be seen that the lattice constant of both ZnO-like and MgO-like phase decreases with increasing x value. This is due to the smaller ion radius of Mg compared to that of Zn. For cubic MgZnO, the lattice constant decreases from 4.251 to 4.240 Å, which indicates that lattice constant of $Mg_xZn_{1-x}O$ is gradually close to that of cubic MgO. In Figure 2(b), when $x \leqslant 0.51$, the FWHMs of hexagonal MgZnO (002) peak increase monotonously with increasing x values. In hexagonal MgZnO alloys, the increase of Mg content may induce serious lattice deformation or disorder due to the composition fluctuations[10], which may be the reason for the broadening of the FWHMs of the (002) diffraction peaks shown in Figure 2(b). For cubic MgZnO, the FWHM of the (111) diffraction peaks decreases rapidly with increasing x from 0.44 to 0.65. As discussed in Figure 1, MgZnO alloy has accomplished a crystal phase transition from hexagonal to cubic when x is above 0.65. Thus, the decrease in the FWHM of cubic MgZnO (111) peak indicates that the crystal structure of cubic MgZnO alloy is improved when the composition of the alloy approaching MgO.

Room-temperature absorption spectra of the samples are shown in Figure 3. All the samples are highly transparent in the visible region and have sharp absorption edges in the UV region. Obviously, for sample D (x=0.44), two absorption edges can be observed, in which the absorption in the lower energy side is from the band-edge absorption of hexagonal MgZnO, while the one at higher energy side is from that of cubic MgZnO. However, for the mixed-phase sample E (x=0.51), only one absorption edge related to cubic MgZnO is observed, which is in good agreement with the
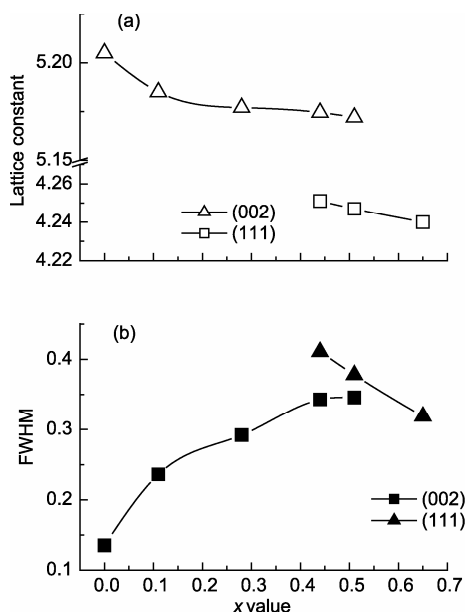
Figure 2 The lattice constants and FWHMs of the $Mg_xZn_{1-x}O$ (002) peak and (111) peak at different x values.

result of very weak MgZnO (002) diffraction peak observed in XRD spectrum. The optical band gap energy (E_g) of the samples can be calculated, assuming that MgZnO alloys obey the following equation [11]: $\alpha = (A/h\nu)(h\nu - E_g)/2$, where α is the absorption coefficient, A is a constant and $h\nu$ is a photon energy. By plotting $(\alpha h\nu)^2$ vs $h\nu$ and extrapolating the linear portion to $\alpha = 0$, the corresponding band gap can be obtained, and the results are plotted in Figure 4. The open circles (○) denote the samples with hexagonal structure, and the soled circles (●) denote the samples with cubic structure. For sample A ($x=0$), the band gap energy is 3.38 eV, similar to that of ZnO bulk (3.37 eV). It is clearly seen from Figure 4 that the band gap increases linearly with Mg content in two different sections, which can be expressed by the following two equations:

$$E_g (Mg_xZn_{1-x}O) = 3.384+1.705x \text{ (for hexagonal-phase } 0 \leqslant x \leqslant 0.44),$$
$$(1)$$

$$E_g (Mg_xZn_{1-x}O) = 3.376+3.051x \text{ (for cubic-phase } 0.44 \leqslant x \leqslant 0.65).$$
$$(2)$$

Eqs. (1) and (2) are in agreement with the results of theoretical calculation made by Chen and his co-workers via the detailed transmission profile method [12]. The above equations are useful to determining the band gap of MgZnO alloys. In addition, a band tail at low energy is observed in the absorption spectra of samples E and F, which is labeled as p and q. From the location of the tail, it is concluded that p and q are related to the defect level of cubic MgO, and the intensity of q is stronger than that of p, which indicates that the defect density increases with increasing Mg content.

The effect of Mg content on the crystallization of $Mg_xZn_{1-x}O$ films is also studied by Raman scattering spectra. Except for sample F, all the samples show intense
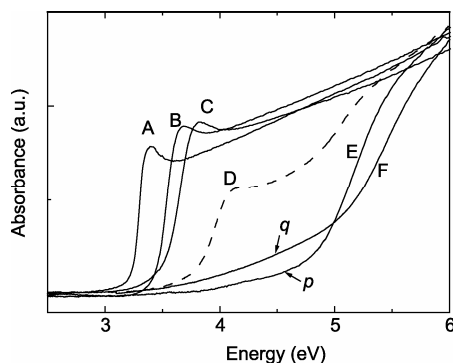

Figure 3 The absorption spectra of samples A, B, C, D, E and F. The absorption in low energy band tail of samples E and F are labeled as p and q.
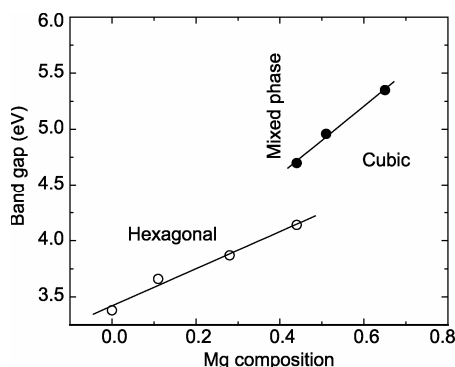

Figure 4 The dependence of the band gap of the MgZnO alloy films on Mg content. Solid lines represent the fitted results from the linear interpolation method.

multi-phonon peaks in the range from 200 to 2500 cm^{-1}. Although the multiple phonon scattering processes have been observed in ZnO thin films [13–16], resonant Raman spectra of MgZnO thin films, to our knowledge, have not been reported up to now. Figure 5(a) shows the typical resonant Raman spectra of samples A and C. The Raman spectrum of sample A is composed of four sharp lines at 583.6, 1164.6, 1745.7 and 2327.1 cm^{-1}, which are from the 1st, 2nd, 3rd, and 4th longitudinal optical (LO) phonons of ZnO wurtzite structure, respectively. This result is consistent with previously reported Raman shift of ZnO bulk crystal and thin films [13–15]. For MgZnO alloy thin films, a typical Raman spectrum of sample C is also shown in Figure 5(a). Compared with the sample A, all the four LO modes are observed. It can be seen that the difference of n-order Raman peaks is very close to 37.5 n ($n = 1, 2, 3, 4$). Actually, the first- and second-order Raman lines in cubic MgO have been reported in the previous work [16]. However, no Raman lines from MgO-like LO phonons are observed in the mixed- and cubic-phased MgZnO alloy samples. Only ZnO-like mode is observed in the MgZnO alloy thin films, indicating very strong resonance enhancement effect in the incident photon energy of 3.81 eV. In order to study the effect of Mg content on the position and FWHM of the Raman peaks, the dependence of the 1-LO center frequencies and FWHM on x value is given in Figure 5(b).

With Mg content increasing from 0 to 0.51, the FWHM of 1-LO phonon peak broadens from 22.9 to 69.2 cm^{-1}, which can be attributed to the increase of lattice disorder and deformation due to the incorporation of Mg^{2+} into ZnO lattice. On the other band, it can be seen from Figure 5 (b) that the position of 1-LO increases from 583.6 to 629.2 cm^{-1}. Because Mg has a smaller ionic radius and a larger electronegative than those of Zn, the bond length of Mg-O is smaller than that of Zn-O. When Mg^{2+} ions are introduced in ZnO lattice, the phonon energy will increase monotonously with increasing Mg content. When $x \leqslant 0.28$, we find that a linear function can be used to express the Raman shift of ZnO-like 1-LO phonon in Mg$_x$Zn$_{1-x}$O alloys, as shown in Figure 5(b):

$$\omega(\text{ZnO-like})=583.3+143.6x(0 \leqslant x \leqslant 0.28). \qquad (3)$$

However, when $x \geqslant 0.28$, the increase of 1-LO zone-center frequency slows down. While the FWHM of 1-LO Raman peak increases with the increase of the Mg content. The results are explained as follows: Firstly, the incorporation of Mg^{2+} ions in ZnO lattice is decreased relatively due to existence of local MgO-rich regions in Mg$_x$Zn$_{1-x}$O alloys with $x \geqslant 0.28$. Secondly, the Raman line becomes less-resonant due to the further broadening of band gap. Similar result has been reported by Demangeot et al. in Al$_x$Ga$_{1-x}$N alloy [17]. With further increasing Mg content to 65%, no Raman peak can be detected due to the crystal structure transition from hexagonal to cubic phases and the excitation energy deviation from resonant condition.

3   Conclusions

The structural and optical properties of Mg$_x$Zn$_{1-x}$O (x=0, 0.11, 0.28, 0.44, 0.51, and 0.65) films are characterized by XRD, optical absorption and Raman scattering. It is found that when $x \leqslant 0.28$, MgZnO alloys keeps single-phased hexagonal structure. When x is increased to 0.44, a phase separation is observed. When x equals 0.65, the sample has completed the transition from wurtzite structure to cubic structure. The multiple-order Raman scattering originating from ZnO-like LO phonons are observed. The position of ZnO-like LO phonons is blueshifted with the increase of the Mg composition. The broadening of the 1-LO phonon scattering peaks is assigned to the increase of lattice disorder and deformation due to the incorporation of Mg^{2+} into the ZnO lattice.

1   Bagnall D M, Chen Y F, Shen M Y, et al. Room-temperature excitonic stimulated emission from zinc oxide epilayers grown by plasma-assisted MBE. J Crystal Growth, 1998, 184-185: 605–609

2   Chen Y F, Ko H J, Hong S K, et al. Layer-by-layer growth of ZnO epilayer on Al$_2$O$_3$(0001) by using a MgO buffer layer. Appl Phys Lett, 2000, 76: 559–561

3   Gruber Th, Kirchner C, Kling R, et al. ZnMgO epilayers and ZnO–ZnMgO quantum wells for optoelectronic applications in the blue and UV spectral region. Appl Phys Lett, 2004, 84: 5359–5361

4   Ohtomo A, Kawasaki M, Ohkubo I, et al. Structure and optical properties of ZnO/Mg$_{0.2}$Zn$_{0.8}$O superlattices. Appl Phys Lett, 1999, 75: 980–982

5   Sarver J F, Katnack F L, Hummel F A. Phase equilibria and manganese-activate fluorescence in the system Zn$_3$(PO$_4$)$_2$–Mg$_3$(PO$_4$)$_2$. J Electrochem Soc, 1959,106:960

6   Park W I, Yi G C, Jang H M. Metalorganic vapor-phase epitaxial growth and photoluminescent properties of Zn$_{1-x}$Mg$_x$O ($0 \leqslant x \leqslant 0.49$) thin films. Appl Phys Lett, 2001, 79: 2022–2024

7   Koike K, Hama K, Nakashima I, et al. Molecular beam epitaxial growth of wide bandgap ZnMgO alloy films on (111)-oriented Si substrate toward UV-detector applications. J Crystal Growth, 2005, 278: 288–292

8   Takagi T, Tanaka H, Fujita S, et al. Molecular beam epitaxy of high magnesium content single-phase wurzite Mg$_x$Zn$_{1-x}$O alloys (x similar or equal to 0.5) and their application to solar-blind region photodetectors. Jpn J Appl Phys, 2003, 42: L401–L403

9   Sharma A K, Narayan J, Muth J F, et al. Optical and structural properties of epitaxial Mg$_x$Zn$_{1-x}$O alloys. Appl Phys Lett, 1999, 75: 3327–3329

10 Muthukumar S, Zhong J, Chen Y, et al. Growth and structural analysis of metalorganic chemical vapor deposited (11(2)over-bar0) Mg$_x$Zn$_{1-x}$O ($0 < x < 0.33$) films on (01(1)over-bar2) R-plane Al$_2$O$_3$ substrates. Appl Phys Lett, 2003, 82: 742–744

11 Janusz M P. Absorption edge of Zn$_3$P$_2$. Phys Rev B, 1982, 26: 4711–4713

12 Chen J, Shen W Z, Chen N B, et al. The study of composition non-uniformity in ternary Mg$_x$Zn$_{1-x}$O thin films. J Phys: Condens Matter, 2003, 15: L475–L482

13 Zhang X T, Liu Y C, Zhang L G, et al. Structure and optically pumped lasing from nanocrystalline ZnO thin films prepared by thermal oxidation of ZnS thin films. J Appl Phys, 2002, 92: 3293– 3298

14 Scott J F. UV Resonant Raman Scattering in ZnO. Phys Rev B, 1970, 2: 1209–1211

15 Ma J G, Liu Y C, Shao C L, et al. Formation and luminescence of ZnO nanoparticles embedded in MgO films. Phys Rev B, 2005, 71: 125430

16 Ishikawa K, Fujima N, Komura H. First-order raman scattering in MgO microcrystals. J Appl Phys, 1985, 57: 974–975

17 Demangeot F, Frandon J, Renucci M A. Far UV resonant Raman scattering in hexagonal Ga$_{1-x}$Al$_x$N alloys. Solid State Comm, 1999, 109: 519–523
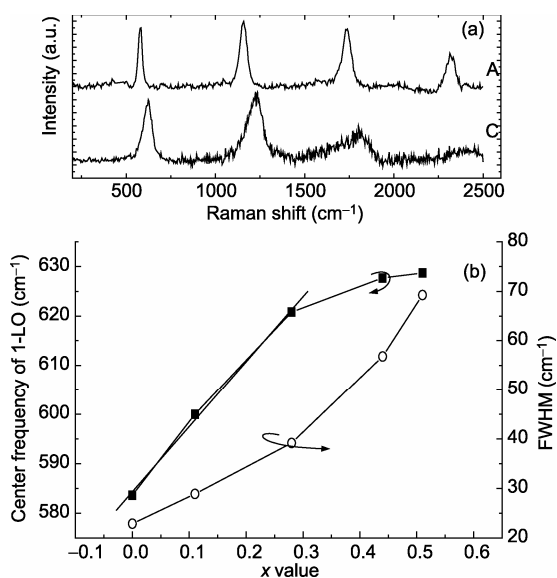
Figure 5   (a) Raman spectra of samples A and C in the range from 200 to 2500 cm^{-1} and (b) the center frequencies and FWHMs of Raman scattering peaks for 1-LO phonons as a function of Mg contents (x value).